COMMUNICATIONS IN COMPUTATIONAL PHYSICS
Vol. **1**, No. 6, pp. 984-1009

Commun. Comput. Phys.
December 2006

On a Fast Integral Equation Method for Diffraction Gratings

A. Rathsfeld[1], G. Schmidt[1,*] and B. H. Kleemann[2]

[1] *Weierstrass Institute for Applied Analysis and Stochastics, Mohrenstr. 39, 10117 Berlin, Germany.*
[2] *Carl Zeiss AG, Corporate Research and Technology, Optical Design, 73446 Oberkochen, Germany.*

Received 30 November 2005; Accepted (in revised version) 8 May 2006

Abstract. The integral equation method for the simulation of the diffraction by optical gratings is an efficient numerical tool if profile gratings determined by simple cross-section curves are considered. This method in its recent version is capable to tackle profile curves with corners, gratings with thin coated layers, and diffraction scenarios with unfavorably large ratio period over wavelength. We discuss special implementational issues including the efficient evaluation of the quasi-periodic Green kernels, the quadrature algorithm, and the iterative solution of the arising systems of linear equations. Finally, as an example we present the simulation of echelle gratings which demonstrates the efficency of our approach.

Key words: Diffraction gratings; integral equation method; preconditioning.

1 Introduction

For the numerical simulation of diffraction by optical gratings, several methods have been proposed, among them differential and integral methods, methods based on Rayleigh or eigenmode expansions, finite element or finite difference methods and methods of analytical continuation (cf., e.g., the Rigorous Coupled Wave Analysis [19], the C-Method [6], and the Finite Element Methods [2,3,8,27]). However, if the cross section of the grating geometry can be described by a small number of interface curves, then the approximation of the scattered electromagnetic field by an integral equation method is recommended. Integral equation methods are robust, reliable, and efficient. Such methods for calculating field components and efficiencies have been developed by e.g. Maystre, Pomp, Chen, Friedman,

*Correspondence to: G. Schmidt, Weierstrass Institute for Applied Analysis and Stochastics, Mohrenstr. 39, 10117 Berlin, Germany. Email: schmidt@wias-berlin.de

Prather et.al., Popov et.al., Yeung, Barouch, Goray, Sadov, and Kleemann (cf. [5, 12, 13, 18, 20, 22, 23, 29]).

Integral equation methods are well suited for the simulation of profile gratings with profile curves of arbitrary shape (cf. [13]). The grating materials can be dielectric or conducting, and profile gratings with coated layers can be treated as well (cf. [12, 20, 22] and the treatment of large numbers of layers in [11]). If the integrals occurring in the method are approximated by properly chosen quadrature rules, then coated layers with extremely small thickness are admissible. Even corners in the profile curve do not cause serious problems as long as the singular behavior of the electromagnetic field at the corner points is taken into account by the right discretization of the integral equations. More challenging is the treatment of gratings with large ratios period (grating constant) over wavelength. Such examples usually require numerical algorithms with large numbers of degrees of freedom, i.e., long computing times and huge storage capacities. Note, however, that surprisingly good results have been reported for the unconventional Modified Integral Method by Goray [10].

Integral equation methods can be considered as a special case of the so-called boundary element methods applied to boundary value problems for the elliptic Helmholtz equation. Consequently, the standard boundary element techniques can be utilized for the grating problems as well. This includes the choice of the discretization scheme and the quadrature rules and the adaption to corners and thin layers. Unfortunately, high ratios period over wavelength result in large wavenumbers which makes the fast iterative solution of the arising linear systems of equations or the implementation of fast methods like fast multipole or wavelet algorithms difficult. Though to our knowledge no attempt has been made to apply the fast boundary element techniques, we believe that they will be useful to design faster integral equation methods for gratings. Finally, let us stress one particularity of the grating problems in comparison to other boundary elements. The kernel functions are quasi-periodic Green's functions represented as infinite sums or integrals. Therefore, the kernel evaluation consumes a lot of computing time, and a fast but accurate evaluation algorithm is often the essential point in an efficient realization of the integral equation method (cf. the contributions by Sadov [25] and Linton [15]).

The subject of the present paper is to describe the recent improvements in the implementation of the integral equation package IESMP of the Carl Zeiss AG in Germany. These improvements enables IESMP to treat gratings with large ratios period over wavelength illuminated under large angles of incidence. Efficiencies of the reflected light in high orders can be determined. In addition, edges (corners of the profile curve in the cross section) and thin dielectric layers can be treated. For example, aluminum echelle gratings with aluminum oxide layers can be simulated. Following Pomp [20], we describe the integral equations for coated gratings and the numerical method in Section 2. In particular, section 2.4 contains some comments on the improved numerical scheme including a mesh grading at the corners. In Section 3.1 we present a new efficient way for the evaluation of the kernel functions inspired by Linton [15]. The new quadrature algorithm is given in Section 3.2, and the iterative solution of the discretized integral equations is discussed in

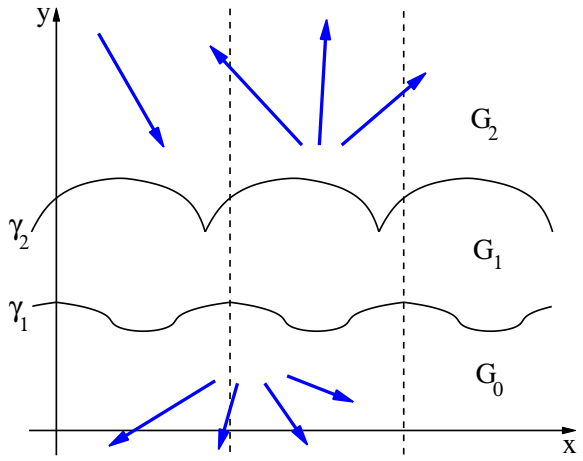

Figure 1: Cross-section of a coated grating.

Section 4. Finally, an example is presented in Section 5.

2 Integral equations and their numerical discretization

2.1 Diffraction problem for optical gratings

A one-dimensional grating is a structure on a planar surface which is periodic in one surface direction and constant in the other. For example, this can mean lots of parallel grooves on the surface of an optical device which, additionally, may be coated. The cross section of a coated diffraction grating, which is periodic in x and homogeneous in z direction, is depicted in Fig. 1. The substrate in domain $G_0 \times \mathbb{R}$ is coated with some optical material, which fills the domain $G_1 \times \mathbb{R}$. From the superstrate $G_2 \times \mathbb{R}$ the structure is illuminated by an electromagnetic plane wave which is reflected and, possibly, transmitted in a finite number of outgoing plane waves. We consider the case of classical TE and TM polarization, where the direction of the wave vector of the incoming wave is in the (x, y)-plane. Then the wave vectors of the diffracted waves are located in the same (x, y)-plane, and the TE and TM diffraction problems can be described by transmission problems for the Helmholtz equation in $\mathbb{R}^2$ as follows.

We denote the period of the grating by d, the frequency of the incoming wave by ω and the wavelength by $\lambda = 2\pi/\omega$. Moreover, we denote the electric permittivity constant of the material in $G_j \times \mathbb{R}$, $j = 0, 1, 2$, by ϵ_j. We assume that the optical materials are non-magnetic and denote the permeability of vacuum by μ. For notational convenience, we scale the geometrical dimensions by a factor of $2\pi/d$ such that the structure becomes 2π-periodic in x-direction. In the case of TE resp. TM polarization the electric resp. magnetic part of the incoming wave is parallel to the z-axis and the underlying time-harmonic Maxwell system can be reduced to the Helmholtz equation for the z-component u of the

total electric resp. magnetic field

$$\Delta u_j + k_j^2 u_j = 0\,, \quad \text{in} \quad G_j\,,\ j = 0,1,2\,. \tag{2.1}$$

Additionally, the u_j satisfy transmission conditions on the interfaces $\gamma_j = \overline{G_{j-1}} \cap \overline{G_j}$, $j = 1, 2$,

$$u_{j-1}|_{\gamma_j} = u_j|_{\gamma_j}\,,\ \partial_n u_{j-1}|_{\gamma_j} = q_j \partial_n u_j|_{\gamma_j}\,, \tag{2.2}$$

with the constants

$$q_j = \begin{cases} 1\,, & \text{TE polarization,} \\ k_{j-1}^2/k_j^2\,, & \text{TM polarization.} \end{cases}$$

Here and in the following the normal n to the interface γ_j is pointing into G_j and ∂_n denotes differentiation in the direction of n. Further, we assume that the coated layer domain G_1 is simply connected, i.e. the two profile curves γ_1 and γ_2 have a positive distance.

The wave numbers k_j in (2.1) are given by

$$k_j = \frac{d}{\lambda}\,\nu_j\,, \quad \nu_j := c\,\sqrt{\mu\epsilon_j} \tag{2.3}$$

where c is the speed of light and where the complex-valued material parameter ν_j is the optical index of the material in G_j. For dielectric materials there holds $\nu > 0$, in particular in vacuum $\nu = 1$, whereas the case $\operatorname{Im}\nu > 0$ accounts for materials absorbing energy. In the following we suppose

$$\nu_2 > 0\,,\ \operatorname{Re}\nu_j > 0\,,\ \operatorname{Im}\nu_j \geq 0\,,\ j = 0,1\,, \tag{2.4}$$

which is satisfied by all relevant materials.

The incoming plane wave is a solution of equation (2.1) in G_2 and therefore of the form

$$u^i(x,y) = p\,e^{i(\alpha x - \beta y)}\,, \quad (\alpha,\beta) := k_2(\sin\theta, \cos\theta)$$

with the angle of incidence θ, $|\theta| < \pi/2$, and with a given amplitude factor $p > 0$. By physical considerations the functions u_j are supposed to be α quasiperiodic, i.e.

$$u_j(x + 2\pi, y) = u_j(x,y)\,e^{i\alpha 2\pi}\,.$$

Above and below the grating structure the outgoing wave condition is required

$$\begin{aligned} u_2 - u^i &= \sum_{n\in\mathbb{Z}} A_n^+ e^{i\alpha_n x + i\beta_n^+ y}\,, \quad y > \max\{y : (x,y) \in \gamma_2\}\,, \\ u_0 &= \sum_{n\in\mathbb{Z}} A_n^- e^{i\alpha_n x - i\beta_n^- y}\,, \quad y < \min\{y : (x,y) \in \gamma_1\}\,. \end{aligned} \tag{2.5}$$

where $A_n^\pm \in \mathbb{C}$ are the Rayleigh coefficients of u_2 and u_0, $\alpha_n := \alpha + n$, and the complex values $\beta_n^\pm = \beta_n^\pm(\alpha)$ are defined as

$$\beta_n^+ := \sqrt{k_2^2 - \alpha_n^2}\,,\ \beta_n^- := \sqrt{k_0^2 - \alpha_n^2} \tag{2.6}$$

with $\operatorname{Im}\beta_n^{\pm} \geq 0$. Since the $\beta_n^{\pm}$ are real for at most finitely many n, there is only a finite number of propagating plane waves in the sums of (2.5).

Under the assumption that the two curves $\gamma_j = \overline{G_{j-1}} \cap \overline{G_j}$, $j = 1, 2$, are Lipschitz, the following existence and uniqueness results for the diffraction problem (2.1), (2.2), (2.5) are valid (cf. [1, 2, 4, 9]):

- In both cases, TE and TM polarization, the diffraction problem has at least one solution which is smooth outside the surface profiles and belongs to the Sobolev space H^2_{loc} for TE resp. H^1_{loc} for TM polarization.
- In both cases, TE and TM polarization, the solution set is an at most finite dimensional affine space.
- If $\operatorname{Im}\nu_j > 0$ for $j = 2$ or 3, then the solution of (2.1), (2.2), (2.5) is unique.
- The TE problem has a unique solution if the y components n_j^y of the normal vectors n_j to the curves γ_j satisfy $n_j^y \geq 0$ and if the refractive indices ν_j satisfy $\nu_1 \leq \nu_2 \leq \nu_3$.

The integral equation approach of the present paper, which has been introduced in [20], transforms the problem (2.1), (2.2), (2.5) into a system of two integral equations over the profile curves (cf. the subsequent Equation (2.20)).

2.2 Integral formulation

The integral representations for α quasi–periodic solutions of the Helmholtz equation are based on potentials including quasi–periodic fundamental solutions as kernel functions. We suppose $k \neq 0$ and set $\alpha_n := \alpha + n$, and $\beta_n := \sqrt{k^2 - \alpha_n^2}$, $n \in \mathbb{Z}$ with $\operatorname{Im}\beta_n \geq 0$. The fundamental solution is given by

$$\Psi_k(x,y) := \frac{i}{4} \sum_{n\in\mathbb{Z}} H_0^{(1)}\Big(k\sqrt{(x-2\pi n)^2+y^2}\Big) e^{2\pi i n\alpha} = \frac{i}{4\pi} \sum_{n\in\mathbb{Z}} \frac{e^{i\alpha_n x + i\beta_n |y|}}{\beta_n}\,, \tag{2.7}$$

where $H_0^{(1)}$ is the first Hankel function of order zero. If one of the denominators β_n in (2.7) is zero, then the corresponding term in the last series must be replaced by $ie^{inx}(C + |y|)$, where C is an arbitrary constant. In the following we will always assume that $\beta_n \neq 0$. Then the series in (2.7) converges uniformly over compact subsets of the set $\{(x,y) : |x| \leq \pi\}\backslash\{(0,0)\}$ and the difference $\Psi_k(x,y) - \log(x^2+y^2)/2\pi$ is smooth. More precisely, the difference is twice continuously differentiable for $x^2 + y^2 > 0$ and the second order derivatives are bounded by constant times $\log(x^2+y^2)$ for x and y tending to zero (cf. [7], Section 3.5).

The profile curves γ_j, $j = 1, 2$, are supposed to be continuous, piecewise differentiable and without cusps, i.e. the angle between adjacent tangents at corner points of γ_j is strictly between 0° and 360°. We denote the restriction of γ_j to the strip $\{(x,y) : 0 \leq x \leq 2\pi\}$ by Γ_j . By assumption $\Gamma_1 \cap \Gamma_2 = \emptyset$. The single and double layer potentials over Γ_j are the

contour integrals

$$V_{\Gamma_j,k}\varphi(P) := -\int_{\Gamma_j} \Psi_k(P-Q)\,\varphi(Q)\,\mathrm{d}s_Q\,, \quad K_{\Gamma_j,k}\varphi(P) := \int_{\Gamma_j} \partial_{n_Q}\Psi_k(P-Q)\,\varphi(Q)\mathrm{d}s_Q\,.$$

Like above ∂_n is the differentiation in the direction of the normal to Γ_j pointing into G_j. The additional index Q in ∂_{n_Q} indicates the normal derivative with respect to the point Q.

In accordance with the classical potential formulas for solutions of the Helmholtz equation satisfying the outgoing wave conditions, the quasi–periodic solutions u_0 and $u_2 - u^i$ can be represented in the form

$$u_0(P) = -V_{\Gamma_1,k_0}\Big(\partial_n u_0|_{\Gamma_1}\Big)(P) - K_{\Gamma_1,k_0}\Big(u_0|_{\Gamma_1}\Big)(P)\,, \qquad P\in G_0\,, \quad (2.8)$$

$$\left[u_2-u^i\right](P) = V_{\Gamma_2,k_2}\Big(\partial_n\left[u_2-u^i\right]|_{\Gamma_2}\Big)(P) + K_{\Gamma_2,k_2}\Big(\left[u_2-u^i\right]|_{\Gamma_2}\Big)(P)\,, \quad P\in G_2\,. \quad (2.9)$$

For the quasi–periodic solution u_1 to the Helmholtz equations in G_1, we choose the potential representation

$$u_1(P) = V_{\Gamma_1,k_1}w_1(P) + V_{\Gamma_2,k_1}w_2(P)\,, \qquad P\in G_1\,, \quad (2.10)$$

with yet unknown densities w_1 and w_2. Taking the limits as the point P tends to the curves Γ_j, the well known jump relations for potentials provide us with two integral equations on Γ_j.

Indeed, if we indicate the limits for $P\in G_{j-1}$ resp. $P\in G_j$ tending to a boundary point at Γ_j in normal direction by the upper index $+$ resp. $-$, then

$$\big(V_{\Gamma_j,k}\varphi\big)^+(P) = \big(V_{\Gamma_j,k}\varphi\big)^-(P) = V_{jj,k}\varphi(P)\,,$$

where we denote

$$V_{jm,k}\varphi(P) := -\int_{\Gamma_m} \Psi_k(P-Q)\,\varphi(Q)\,\mathrm{d}s_Q\,, \quad P\in\Gamma_j\,. \quad (2.11)$$

The boundary limits of the double layer potential from the two sides of Γ_j take the values

$$\big(K_{\Gamma_j,k}\varphi\big)^+(P) = K_{jj,k}\varphi(P)+\Big(1-\delta_j(P)\Big)\varphi(P),\ \big(K_{\Gamma_j,k}\varphi\big)^-(P) = K_{jj,k}\varphi(P)-\delta_j(P)\varphi(P),$$

where the function $\delta_j(P)\in(0,1)$ denotes the normalized interior angle of G_j at the boundary point $P\in\Gamma_j$, i.e., $\delta_j(P)$ is the interior angle of G_j measured in arc length divided by 2π. Obviously, $\delta_j(P)=1/2$ if $P\in\Gamma_j$ is not a corner point. The integral operator $K_{jm,k}$ is defined by

$$K_{jm,k}\varphi(P) := \int_{\Gamma_m} \partial_{n_Q}\Psi_k(P-Q)\,\varphi(Q)\,\mathrm{d}s_Q\,, \quad P\in\Gamma_j\,.$$

Finally, for $P \in \Gamma_j$ not a corner, the normal derivative of the single layer potential has the limits

$$\big(\partial_n V_{\Gamma_j,k}\varphi\big)^+(P) = -L_{jj,k}\varphi(P) + \frac{1}{2}\varphi(P)\,, \quad \big(\partial_n V_{\Gamma_j,k}\varphi\big)^-(P) = -L_{jj,k}\varphi(P) - \frac{1}{2}\varphi(P)\,,$$

where we use the notation

$$L_{jm,k}\varphi(P) := \int_{\Gamma_m} \partial_{n_P}\Psi_{k_j}(P-Q)\,\varphi(Q)\,\mathrm{d}s_Q\,, \qquad P \in \Gamma_j\,.$$

Thus we obtain the relations

$$u_0|_{\Gamma_1} = -V_{11,k_0}\Big(\partial_n u_0|_{\Gamma_1}\Big) - \Big(K_{11,k_0} - \delta_1\Big)\Big(u_0|_{\Gamma_1}\Big), \tag{2.12}$$

$$u_1|_{\Gamma_1} = V_{11,k_1}w_1 + V_{12,k_1}w_2\,, \tag{2.13}$$

$$\partial_n u_1|_{\Gamma_1} = \Big(1/2 - L_{11,k_1}\Big)w_1 - L_{12,k_1}w_2\,, \tag{2.14}$$

$$u_1|_{\Gamma_2} = V_{21,k_1}w_1 + V_{22,k_1}w_2\,, \tag{2.15}$$

$$\partial_n u_1|_{\Gamma_2} = -L_{21,k_1}w_1 - \Big(1/2 + L_{22,k_1}\Big)w_2\,, \tag{2.16}$$

$$\big[u_2 - u^i\big]\,|_{\Gamma_2} = V_{22,k_2}\Big(\partial_n\big[u_2 - u^i\big]\,|_{\Gamma_2}\Big) + \Big(K_{22,k_2} + (1-\delta_2)\Big)\Big(\big[u_2 - u^i\big]\,|_{\Gamma_2}\Big). \tag{2.17}$$

Equation (2.12) can be written in the form

$$V_{11,k_0}\Big(\partial_n u_0|_{\Gamma_1}\Big) + \Big(K_{11,k_0} + (1-\delta_1)\Big)\Big(u_0|_{\Gamma_1}\Big) = 0\,.$$

Applying the transmission conditions $u_0 = u_1$ and $\partial_n u_0 = q_1\partial_n u_1$ over Γ_1 and substituting (2.13) and (2.14), we arrive at

$$q_1 V_{11,k_0}\Big((1/2 - L_{11,k_1})w_1 - L_{12,k_1}w_2\Big) + \Big(K_{11,k_0} + (1-\delta_1)\Big)\Big(V_{11,k_1}w_1 + V_{12,k_1}w_2\Big) = 0\,. \tag{2.18}$$

On the other hand, from (2.17) we derive the relation

$$V_{22,k_2}\Big(\partial_n u_2|_{\Gamma_2}\Big) + \Big(K_{22,k_2} - \delta_2\Big)\Big(u_2|_{\Gamma_2}\Big) = V_{22,k_2}\Big(\partial_n u^i|_{\Gamma_2}\Big) + \Big(K_{22,k_2} - \delta_2\Big)\Big(u^i|_{\Gamma_2}\Big) = -u^i\,,$$

which together with the transmission conditions $u_1 = u_2$ and $\partial_n u_1 = q_2\partial_n u_2$ on Γ_2 and with the help of (2.15), (2.16) implies the equation

$$\frac{1}{q_2}V_{22,k_2}\Big(-L_{21,k_1}w_1 - (1/2 + L_{22,k_1})w_2\Big) + \Big(K_{22,k_2} - \delta_2\Big)\Big(V_{21,k_1}w_1 + V_{22,k_1}w_2\Big) = -u^i\,. \tag{2.19}$$

Hence, we obtain the system (2.18), (2.19) of integral equations for the unknown densities w_j which can be written as

$$\begin{pmatrix} A_{1,1} & A_{1,2} \\ A_{2,1} & A_{2,2} \end{pmatrix} \begin{pmatrix} w_1 \\ w_2 \end{pmatrix} = \begin{pmatrix} 0 \\ u^i \end{pmatrix} \tag{2.20}$$

with the operators

$$\begin{aligned} A_{1,1} &:= q_1 V_{11,k_0}\Big(1/2 - L_{11,k_1}\Big) + \Big(K_{11,k_0} + (1-\delta_1)\Big)V_{11,k_1}\,, \\ A_{1,2} &:= -q_1 V_{11,k_0} L_{12,k_1} + \Big(K_{11,k_0} + (1-\delta_1)\Big)V_{12,k_1}\,, \\ A_{2,1} &:= \frac{1}{q_2} V_{22,k_2} L_{21,k_1} - \Big(K_{22,k_2} - \delta_2\Big)V_{21,k_1}\,, \\ A_{2,2} &:= \frac{1}{q_2} V_{22,k_2}\Big(1/2 + L_{22,k_1}\Big) - \Big(K_{22,k_2} - \delta_2\Big)V_{22,k_1}\,. \end{aligned} \tag{2.21}$$

Note that system (2.20) has first been obtained in [20] and is more efficient than other integral formulations proposed, e.g., in [18, 22], where the computation of the inverse of certain integral operators is required.

2.3 Periodic integral operators

For the implementation it is convenient to use a periodic setting of the integral equations. We choose 2π-periodic parametrizations of the curves Γ_j, $j = 1, 2$,

$$\gamma_j(t) := \Big(X_j(t), Y_j(t)\Big), \quad X_j(t+2\pi) \;=\; X_j(t) + 2\pi, \quad Y_j(t+2\pi) \;=\; Y_j(t)\,, \tag{2.22}$$

and denote $\sigma_j(t) := \sqrt{X_j'(t)^2 + Y_j'(t)^2}$. We introduce the periodic unknown functions

$$\varphi_j(t) := e^{-i\alpha X_j(t)} w_j\Big(X_j(t), Y_j(t)\Big)\,,$$

and, for $P = (X_j(t), Y_j(t)) \in \Gamma_j$ and $Q = (X_m(s), Y_m(s)) \in \Gamma_m$, we set

$$\hat{e}_{n,k}(t,s) := e_{n,k}\Big(X_j(t) - X_m(s), Y_j(t) - Y_m(s)\Big)\,,$$

where

$$e_{n,k}(x,y) := e^{inx + i\beta_n|y|}\,, \quad \beta_n := \sqrt{k^2 - (n+\alpha)^2}\,.$$

Then we have to solve the system (2.20) with the integral operators $V_{jm,k}$, $K_{jm,k}$, and $L_{jm,k}$, defining $A_{j,k}$ in (2.21), replaced by their periodic counterparts

$$\widetilde{V}_{jm,k}\,\varphi(t) := \frac{1}{4\pi i}\int_0^{2\pi}\sum_{n\in\mathbb{Z}}\frac{\hat{e}_{n,k}(t,s)}{\beta_n}\,\sigma_m(s)\,\varphi(s)\,\mathrm{d}s\,,$$

$$\widetilde{K}_{jm,k}\,\varphi(t) := \frac{1}{4\pi}\int_0^{2\pi}\sum_{n\in\mathbb{Z}}\left(\frac{n+\alpha}{\beta_n}Y_m'(s) - X_m'(s)\,\mathrm{sign}\left(Y_j(t)-Y_m(s)\right)\right)\hat{e}_{n,k}(t,s)\,\varphi(s)\,\mathrm{d}s\,,$$

$$\widetilde{L}_{jm,k}\,\varphi(t) := -\frac{1}{4\pi}\int_0^{2\pi}\sum_{n\in\mathbb{Z}}\left(\frac{n+\alpha}{\beta_n}Y_j'(t) - X_j'(t)\,\mathrm{sign}\left(Y_j(t)-Y_m(s)\right)\right)\hat{e}_{n,k}(t,s)\,\varphi(s)\,\mathrm{d}s\,.$$

2.4 Numerical scheme of discretization

As usual in boundary element methods, there exist several choices for the discretization scheme. The trial space X_N of finite dimension N, where the approximate solution $\varphi_N \in X_N$ to the exact solution $\varphi = \varphi_j$, $j = 1, 2$ is sought, can be the space of trigonometric functions or a space of spline functions. If the unknown solution is known to be smooth, than the trigonometric space exhibits higher order approximation rates. Unfortunately, the basis functions spanning the trigonometric space have global supports. Applying the integral operators to such basis functions results in global integrals. In contrast to this, applying the integral operators to a local basis of spline functions results in local integrals and leads to faster algorithms. In other words, spline methods are often faster.

Aside from the choice of trial functions, the discretization schemes differ also in the way in which the continuous integral equation is converted into a finite dimensional equation. Galerkin methods first restrict the integral operator to the trial space. Then, after applying the operator to a general trial function, they project the resulting function to its best approximation in the trial space. This way the integral operator is replaced by a finite dimensional operator acting in the finite dimensional trial space. Let us denote by B one of the integral operators $\widetilde{V}_{jm,k}$, $\widetilde{K}_{jm,k}$, $\widetilde{L}_{jm,k}$. If P_N is the orthogonal projection of L^2 onto the trial space X_N, then the discretized operator $[B]_N$ of the Galerkin method is defined as

$$[B]_N := P_N B|_{X_N} : X_N \longrightarrow X_N\,.$$

The collocation method applies the integral operator to a general trial function φ_N but, in contrast to Galerkin's method, the result is computed on a finite set of so-called collocation points $\{s_k^{\mathrm{col}} : k = 1, \ldots, N\}$, only. Usually, these collocation points s_k^{col} are the points of a uniform grid. Again a finite dimensional operator results mapping the trial space functions to the integral operator images restricted to the collocation points. The discretized operator $[B]_N$ of the collocation is defined as

$$[B]_N : X_N \ni \varphi_N \mapsto \left(B(\varphi_N)(s_k^{\mathrm{col}})\right)_{k=1}^N\,.$$

Supposing that for each sequence of function values $(f(s_k^{\rm col}))_{k=1}^N$ there is exactly one function $f_N \in X_N$ with $f_N(s_k^{\rm col}) = f(s_k^{\rm col})$, we can identify the sequence $(f(s_k^{\rm col}))_{k=1}^N$ with $f_N \in X_N$. This way $[B]_N$ maps X_N into X_N and the image of φ_N is the unique function in X_N satisfying

$$\big([B]_N\varphi_N\big)(s_k^{\rm col}) = B(\varphi_N)(s_k^{\rm col}),\ k = 1,\ldots,N\,.$$

In general, collocation methods are faster but the convergence rate for Galerkin methods is higher. We note, however, that Galerkin's method and collocation are so-called semi-discrete schemes. The entries of the matrix equations corresponding to the discretized operators still have entries containing analytic integrals. E.g. the collocation discretization of B requires the computation of the integrals $B(\varphi_N)(s_k^{\rm col})$. Hence, Galerkin's method and collocation must be combined with a quadrature algorithm for the computation of these integrals (cf. Section 3.2).

The fastest and fully discrete numerical scheme, however, is the Nyström method where again the integral equations are considered at a set of collocation points, only, and where the integral in the integral operators is approximated by a quadrature rule with the collocation points used as quadrature knots. The Nyström method works well for integral operators with smooth kernel functions.

The first version of the package IESMP (cf. [13,20]) is based on a hybrid discretization scheme. This so-called method of mechanical quadratures is very fast for smooth curves and thick layers. In this case the integral operators except the single layer operators $\widetilde{V}_{jj,k}$ have smooth kernels. The operators $\widetilde{V}_{jj,k}$ are split into the single layer operator over the unit circle corresponding to the Laplace operator and a remainder. Since the action of the single layer operator on the trigonometric trial space is known explicitly, the single layer part is easily discretized by a trigonometric Galerkin scheme. The remainder and all other operators are discretized by a fast Nyström approximation. Unfortunately, the convergence properties deteriorate if corner singularities appear in the solutions of the integral equations and if the Nyström quadrature rules over the uniform collocation points are inaccurate due to thin layers.

To deal with corners in the profile curves, we have introduced meshes of collocation points graded towards the corner points. The grading is defined simply by changing the parametrization in the formulas of Section 2.3. For instance, if $\gamma_j : \mathbb{R} \to \mathbb{C}$ is a smooth parametrization of curve γ_j such that $|\partial_t\gamma_j(t)| > 0$ for all points $\gamma_j(t)$ except the corners and if $|\partial_t\gamma_j(t)| = |\partial_t^2\gamma_j(t)| = 0$ holds at all the corner points, then the corresponding collocation points $\{\gamma_j(2\pi k/N) : k = 1,\ldots,N\}$ are graded towards the corners. The improved discretization scheme for corners is just the collocation method based on these collocation nodes and on spline functions subordinate to this mesh. The splines subordinate to this mesh are piecewise polynomials equal to cubic polynomials between consecutive collocation nodes. Of course, to compute the action of the integral operator on basis spline functions, a clever quadrature rule is needed (cf. Section 3.2). In contrast to the Nyström method, the quadrature rule must depend on the collocation point. Even thin layers can be treated by the same spline collocation if the quadrature rules are adapted (cf. Section

Table 1: Convergence of efficiencies simulating a simple echelle grating.

N	graded mesh		uniform mesh	
	$\text{Effic}_0^{\text{tr}}$	Total Energy	$\text{Effic}_0^{\text{tr}}$	Total Energy
8	79.5335	116.80585	70.1237	98.87362
16	91.1789	99.75135	84.1812	92.76585
32	90.4132	99.43106	88.6170	97.57554
64	90.3557	99.39309	89.7681	98.76689
128	90.3555	99.39521	90.1993	99.22791
256	90.3562	99.39616	90.3350	99.37354
512	90.3564	99.39640	90.3588	99.39901
1024	90.3565	99.39646	90.3580	99.39819

3.2).

As a simple example, we consider a triangular grating of period $1\,\mu$m with an apex angle of 120° and a side angle of 40°. The grating consists of a substrate material with refractive index equal to 1.5 and is coated by a layer of uniform thickness equal to 1 nm with index $\nu = 1.2 + i\,0.2$. The echelle grating is illuminated in TM polarization by light of the wavelength 633 nm under an incidence angle of 60°. We have applied the collocation method with $N = 8$, 16, 32, 64, 128, 256, 512, and 1 024 collocation points at each curve. Hence, the dimension of the system of linear equations to be solved is $2N$. By $\text{Effic}_0^{\text{tr}}$ we denote the transmitted zero order efficiency (angle of radiation 35.26°) and by Total Energy the total rate of transmitted and reflected energy. Table 1 exhibits the convergence of the integral equation method. Moreover, an essential improvement of the convergence for graded meshes can be observed.

3 Computation of integrals

3.1 Ewald's method for the kernel computation

In the old IESMP program package a sophisticated summation method of 5-th order is implemented to accelerate the computation of the integral kernels (cf. [13] and compare [25]). Unfortunately, it has turned out that this approach is not efficient for the second argument y with small modulus $|y|$ (cf. (2.7)), which frequently occur in the quadrature of integrals for graded meshes near corners or for thin layers, i.e., for thin domains G_1. In this case we use the following summation algorithm for the integral kernel which is based on Ewald's method (cf. [15] and [28]).

Consider the infinite series

$$\Psi(x,y) = \frac{i}{4\pi} \sum_{n\in\mathbb{Z}} \frac{e^{inx+i\beta_n|y|}}{\beta_n} \tag{3.1}$$

with $\beta_n := \sqrt{k^2-\alpha_n^2}$ and $\alpha_n := n+\alpha$. Note that $\operatorname{Re}\beta_n$, $\operatorname{Im}\beta_n \geq 0$. Ewald's method is based on the relation

$$\frac{ie^{i\beta_n|y|}}{\beta_n} = \int_0^{a^2} \exp\Big(\beta_n^2 t - \frac{y^2}{4t}\Big)\frac{\mathrm{d}t}{\sqrt{\pi t}} + \frac{i}{2\beta_n}\left(e^{-iy\beta_n}\operatorname{erfc}\Big(-ia\beta_n + \frac{y}{2a}\Big) + e^{iy\beta_n}\operatorname{erfc}\Big(-ia\beta_n - \frac{y}{2a}\Big)\right),$$

which is valid for any $a>0$ and $\beta_n \neq 0$. Here

$$\operatorname{erfc}(z) := \frac{2}{\sqrt{\pi}}\int_z^\infty e^{-t^2}\,\mathrm{d}t$$

is the *complementary error function*. Thus we have $\Psi = \Psi^e + \Psi^w$ with the two sums

$$\Psi^e(x,y) = \frac{1}{4\pi}\sum_{n\in\mathbb{Z}} e^{inx}\int_0^{a^2} e^{\beta_n^2 t - y^2/4t}\frac{\mathrm{d}t}{\sqrt{\pi t}}\,, \tag{3.2}$$

$$\Psi^w(x,y) = \frac{i}{8\pi}\sum_{n\in\mathbb{Z}}\frac{e^{inx}}{\beta_n}\left(e^{-iy\beta_n}\operatorname{erfc}\Big(-ia\beta_n+\frac{y}{2a}\Big) + e^{iy\beta_n}\operatorname{erfc}\Big(-ia\beta_n-\frac{y}{2a}\Big)\right). \tag{3.3}$$

Since $\beta_n^2 = k^2-\alpha_n^2$, the first sum (3.2) takes the form

$$\Psi^e(x,y) = \frac{1}{4\pi}\sum_{n\in\mathbb{Z}} e^{inx}\int_0^{a^2} e^{(k^2-\alpha_n^2)t - y^2/4t}\,\frac{\mathrm{d}t}{\sqrt{\pi t}} = \frac{1}{4\pi}\int_0^{a^2} e^{k^2 t - y^2/4t}\sum_{n\in\mathbb{Z}} e^{-\alpha_n^2 t}e^{inx}\,\frac{\mathrm{d}t}{\sqrt{\pi t}}\,.$$

Poisson's summation formula gives

$$\sum_{n\in\mathbb{Z}} e^{-(\alpha+n)^2 t}e^{inx} = \sqrt{\frac{\pi}{t}}e^{-i\alpha x - x^2/4t}\sum_{m\in\mathbb{Z}} e^{-\pi^2 m^2/t}\,e^{\pi m x/t}\,e^{2\pi i m\alpha}\,,$$

which leads to

$$\Psi^e(x,y) = \frac{e^{-i\alpha x}}{4\pi}\sum_{m\in\mathbb{Z}} e^{2\pi i m\alpha}\int_0^{a^2} e^{k^2 t}e^{-((x-2\pi m)^2+y^2)/4t}\,\frac{\mathrm{d}t}{t}\,. \tag{3.4}$$

Denoting $r_m^2 := (x-2\pi m)^2 + y^2$ and using the series expansion of $e^{\,k^2 t}$ gives

$$\int_0^{a^2} e^{\,k^2 t}e^{-r_m^2/4t}\,\frac{\mathrm{d}t}{t} = \sum_{j=0}^\infty \frac{k^{2j}}{j!}\int_0^{a^2} t^{j-1}\,e^{-r_m^2/4t}\,\mathrm{d}t = \sum_{j=0}^\infty \frac{(ak)^{2j}}{j!}E_{j+1}\Big(\frac{r_m^2}{4a^2}\Big)$$

with the *exponential integral function* E_j of degree j

$$E_j(z) := \int_1^\infty \frac{e^{-zt}}{t^j}\,\mathrm{d}t\,.$$

Thus we obtain the representation

$$\Psi^e(x,y) = \frac{e^{-i\alpha x}}{4\pi}\sum_{m\in\mathbb{Z}} e^{2\pi i m\alpha}\sum_{j=0}^\infty \frac{(ak)^{2j}}{j!}E_{j+1}\Big(\frac{r_m^2}{4a^2}\Big). \tag{3.5}$$

The function Ψ^w can be transformed to a computationally suitable form by using the *scaled complementary error function*

$$\mathrm{w}(z) := e^{-z^2}\,\mathrm{erfc}(-iz) = e^{-z^2}\frac{2}{\sqrt{\pi}}\int_{-iz}^\infty e^{-t^2}\,\mathrm{d}t = \frac{2}{\sqrt{\pi}}\int_0^\infty e^{-t^2}\,e^{2izt}\,\mathrm{d}t\,, \tag{3.6}$$

which has the properties

$$\mathrm{w}(-\overline{z}) = \overline{\mathrm{w}(z)}\,,\quad \mathrm{w}(-z) = 2e^{-z^2} - \mathrm{w}(z)\,,\quad |\,\mathrm{w}(z)| \le 1 \ \text{ for } \operatorname{Im} z \ge 0\,. \tag{3.7}$$

Using

$$e^{\mp iy\beta_n}\mathrm{erfc}\Big(-ia\beta_n \pm \frac{y}{2a}\Big) = e^{a^2k^2}e^{-a^2\alpha_n^2}\,e^{-y^2/4a^2}\,\mathrm{w}\Big(a\beta_n \pm i\frac{y}{2a}\Big),$$

we can write (3.3) in the form

$$\Psi^w(x,y) = \frac{i\,e^{-y^2/4a^2}\,e^{a^2k^2}}{8\pi}\sum_{n\in\mathbb{Z}}\frac{e^{inx}\,e^{-a^2\alpha_n^2}}{\beta_n}\left(\mathrm{w}\Big(a\beta_n + i\frac{y}{2a}\Big) + \mathrm{w}\Big(a\beta_n - i\frac{y}{2a}\Big)\right). \tag{3.8}$$

From (3.7) it can be seen that $|\,\mathrm{w}(z)| = \mathcal{O}(e^{(\operatorname{Im} z)^2-(\operatorname{Re} z)^2})$ if $\operatorname{Im} z < -|\operatorname{Re} z|$. To avoid numerical overflow problems, which may occur if $|y|/a$ is large, we use the relation

$$\mathrm{w}\Big(a\beta_n - i\frac{|y|}{2a}\Big) = 2\,e^{y^2/4a^2}\,e^{-a^2(k^2-\alpha_n^2)}e^{i|y|\beta_n} - \mathrm{w}\Big(-a\beta_n + i\frac{|y|}{2a}\Big) \tag{3.9}$$

obtained from (3.7), which gives

$$\frac{i\,e^{-y^2/4a^2}\,e^{a^2k^2}}{8\pi}\frac{e^{-a^2\alpha_n^2}}{\beta_n}\left(\mathrm{w}\Big(a\beta_n - i\frac{|y|}{2a}\Big) + \mathrm{w}\Big(-a\beta_n + i\frac{|y|}{2a}\Big)\right) = \frac{i}{4\pi}\frac{e^{i|y|\beta_n}}{\beta_n}\,.$$

Introducing the finite set $P := \{n\in\mathbb{Z} : \operatorname{Im}\beta_n + \operatorname{Re}\beta_n < |y|/[2a^2]\}$, the function Ψ^w is decomposed into an exponentially converging series and two finite sums

$$\begin{aligned}\Psi^w(x,y) = \frac{i\,e^{-y^2/4a^2}\,e^{a^2k^2}}{8\pi}\Bigg\{&\sum_{n\in\mathbb{Z}\setminus P}\frac{e^{inx}\,e^{-a^2\alpha_n^2}}{\beta_n}\left(\mathrm{w}\Big(a\beta_n + i\frac{y}{2a}\Big) + \mathrm{w}\Big(a\beta_n - i\frac{y}{2a}\Big)\right)\\ &+\sum_{n\in P}\frac{e^{inx}\,e^{-a^2\alpha_n^2}}{\beta_n}\left(\mathrm{w}\Big(a\beta_n + i\frac{|y|}{2a}\Big) - \mathrm{w}\Big(-a\beta_n + i\frac{|y|}{2a}\Big)\right)\Bigg\} + \frac{i}{4\pi}\sum_{n\in P}\frac{e^{inx}e^{i|y|\beta_n}}{\beta_n}\,.\end{aligned} \tag{3.10}$$

Note that, in the case $y = 0$ which occurs frequently for binary gratings, we obtain the exponentially converging series

$$\Psi^w(x,0) = \frac{i\,e^{a^2k^2}}{4\pi} \sum_{n\in\mathbb{Z}} \frac{e^{inx}\,e^{-a^2\alpha_n^2}}{\beta_n}\,\mathrm{w}\big(a\beta_n\big).$$

The representation $\Psi = \Psi^e + \Psi^w$ is also used for the computation of the gradient of Ψ:

$$(\partial_x + i\alpha)\Psi(x,y) = -\frac{1}{4\pi}\sum_{n\in\mathbb{Z}} \frac{\alpha_n e^{inx+i\beta_n|y|}}{\beta_n}\,, \quad \partial_y\Psi(x,y) = -\frac{1}{4\pi}\sum_{n\in\mathbb{Z}} \mathrm{sign}(y) e^{inx+i\beta_n|y|}\,,$$

which is needed to compute the kernels of the operators $\widetilde{K}$ and $\widetilde{L}$. Since $\partial_z E_j(z) = -E_{j-1}(z)$ with $E_0(z) := e^{-z}/z$, the derivatives of Ψ^e are

$$\begin{aligned}
(\partial_x + i\alpha)\Psi^e(x,y) &= -\frac{e^{-i\alpha x}}{2\pi}\sum_{m\in\mathbb{Z}} (x-2\pi m)\,e^{2\pi i m\alpha}\left(\frac{e^{-r_m^2/4a^2}}{r_m^2} + \sum_{j=1}^{\infty}\frac{(ak)^{2j}}{4a^2 j!}E_j\Big(\frac{r_m^2}{4a^2}\Big)\right),\\
\partial_y\Psi^e(x,y) &= -\frac{y\,e^{-i\alpha x}}{2\pi}\sum_{m\in\mathbb{Z}} e^{2\pi i m\alpha}\left(\frac{e^{-r_m^2/4a^2}}{r_m^2} + \sum_{j=1}^{\infty}\frac{(ak)^{2j}}{4a^2 j!}E_j\Big(\frac{r_m^2}{4a^2}\Big)\right).
\end{aligned} \tag{3.11}$$

The derivatives of Ψ^w are given by

$$\begin{aligned}
(\partial_x + i\alpha)\Psi^w(x,y) = -\frac{e^{-y^2/4a^2}\,e^{a^2k^2}}{8\pi}\Bigg\{ &\sum_{n\in\mathbb{Z}\setminus P}\frac{\alpha_n e^{inx}\,e^{-a^2\alpha_n^2}}{\beta_n}\left(\mathrm{w}\Big(a\beta_n + i\frac{y}{2a}\Big) + \mathrm{w}\Big(a\beta_n - i\frac{y}{2a}\Big)\right)\\
&+ \sum_{n\in P}\frac{\alpha_n e^{inx}\,e^{-a^2\alpha_n^2}}{\beta_n}\left(\mathrm{w}\Big(a\beta_n + i\frac{|y|}{2a}\Big) - \mathrm{w}\Big(-a\beta_n + i\frac{|y|}{2a}\Big)\right)\Bigg\} - \frac{1}{4\pi}\sum_{n\in P}\frac{\alpha_n e^{inx}e^{i|y|\beta_n}}{\beta_n}\,,
\end{aligned} \tag{3.12}$$

and

$$\begin{aligned}
\partial_y\Psi^w(\mathbf{x}) = \frac{e^{-y^2/4a^2}\,e^{a^2k^2}}{8\pi}\,\mathrm{sign}(y)\Bigg\{ &\sum_{n\in\mathbb{Z}\setminus P} e^{inx}\,e^{-a^2\alpha_n^2}\left(\mathrm{w}\Big(a\beta_n + i\frac{|y|}{2a}\Big) - \mathrm{w}\Big(a\beta_n - i\frac{|y|}{2a}\Big)\right)\\
&+ \sum_{n\in P} e^{inx}\,e^{-a^2\alpha_n^2}\left(\mathrm{w}\Big(a\beta_n + i\frac{|y|}{2a}\Big) + \mathrm{w}\Big(-a\beta_n + i\frac{|y|}{2a}\Big)\right)\Bigg\} - \mathrm{sign}(y)\frac{1}{4\pi}\sum_{n\in P} e^{inx}e^{i|y|\beta_n},
\end{aligned} \tag{3.13}$$

where we use the relation

$$\begin{aligned}
&\partial_y\left(e^{-y^2/4a^2}\left(\mathrm{w}\Big(a\beta_n + i\frac{y}{2a}\Big) + \mathrm{w}\Big(a\beta_n - i\frac{y}{2a}\Big)\right)\right)\\
=&\,i\beta_n e^{-y^2/4a^2}\left(\mathrm{w}\Big(a\beta_n - i\frac{y}{2a}\Big) - \mathrm{w}\Big(a\beta_n + i\frac{y}{2a}\Big)\right).
\end{aligned}$$

The numerical calculation of the exponential integral E_j and its derivatives present no problem using a standard routine for E_1 and the known recurrence relations. The scaled complementary error function $\mathrm{w}(z)$ is computed using two different algorithms depending on the value of z, the algorithm 680 from ACM ([21]) and the summation algorithm of [17]. The value of the parameter a should be chosen small enough to ensure the rapid convergence of the series for Ψ^e and its derivatives and large enough to ensure the rapid convergence of the series representations for Ψ^w and its derivatives. After numerical tests we found that the choice $a|k| = 6$ is a good compromise.

3.2 Quadrature algorithm

The concept for the quadrature rules is simple and well known (cf. [26]). Suppose we have to evaluate one of the integrals $\widetilde{V}_{jm,k}\varphi(t)$, $\widetilde{K}_{jm,k}\varphi(t)$, or $\widetilde{L}_{jm,k}\varphi(t)$, from Section 2.3 with a spline basis function φ. We write this integral in the form

$$I := \int_0^{2\pi} k(t,s)\varphi(s)\mathrm{d}s = \int_{\{s\in[0,2\pi]:\,\varphi(s)\neq 0\}} k(t,s)\varphi(s)\mathrm{d}s.$$

Of course, the functions k and φ are periodic with period 2π. The function φ is a piecewise polynomial spline function subordinate to a mesh of collocation points $\{s_n^{\mathrm{col}} : n = 1,\dots,N\}$. The kernel function k is either weakly singular with singularity for s tending to t or almost singular for s tending to t. Weakly singular means $|k(t,s)| \le c\log(t-s)$ and almost singular means either $|k(t,s)| \le c\min\{|t-s|^{-1},\varepsilon^{-1}\}$ or $|k(t,s)| \le c\min\{\log(|t-s|^{-1}),\log(\varepsilon^{-1})\}$, where c is an appropriate positive constant and where ε is a fixed small positive number. The weakly singular case occurs if the single layer integral $I = \widetilde{V}_{jj,k}\varphi(t)$ is computed over the curve Γ_j and if the collocation point corresponding to parameter value t is located on the same curve Γ_j. The almost singular case appears if an integral I is computed over a curve Γ_j and if the collocation point $\gamma_m(t')$ is located on a neighbor curve Γ_m, but extremely close to the support $\{\gamma_j(s) \in [0,2\pi] : \varphi(s) \neq 0\}$ of φ. In this case the almost singular point t is the parameter of the point $\gamma_j(t) \in \gamma_j$ closest to the collocation point $\gamma_m(t')$, and ε is the distance between $\gamma_j(t')$ and $\gamma_j(t)$. A second case of an almost singular integrand appears if the curve of integration Γ_j has corners, if I is the double layer integral $\widetilde{K}_{jj,k}\varphi(t)$ or the adjoint double layer integral $\widetilde{L}_{jj,k}\varphi(t)$, if the collocation point $\gamma_j(t) \in \Gamma_j$ is located in a vicinity of a corner point, and if the support of φ contains points of Γ_j from the other side of the corner. In this case ε is the distance of $\gamma_j(t)$ to the corner point.

To compute the integral I by quadrature, we introduce a quadrature mesh which is geometrically graded towards t, i.e., a mesh $\{s_m^{\mathrm{geo}} : n = 1,\dots,M\}$ such that

$$\begin{aligned}\left\{s_m^{\mathrm{geo}} : m = 1,\dots,M\right\} := \left\{t\right\} &\cup \left\{s = t \pm q^l : l = 1,\dots,L,\ s \in [0,2\pi]\right\} \\ &\cup \left\{s = t \pm q^l \pm 2\pi : l = 1,\dots,L,\ s \in [0,2\pi]\right\},\end{aligned}$$

with an exponent $q \leq 1$ ($q = 0.2$ or $q = 0.3$) and a suitable refinement number L. In the almost singular case, L must be chosen such that $q^L \leq \varepsilon$. For the weakly singular case, L must be determined by numerical tests and depends on the desired accuracy. The geometrically graded mesh $\{s_n^{\rm col} : n = 1, \ldots, N\}$ is a good quadrature mesh for the quadrature points of the piecewise polynomial φ and $\{s_m^{\rm geo} : n = 1, \ldots, M\}$ a good choice to treat the singularity inherent in the kernel function k. Consequently, we form the quadrature mesh by joining the two.

$$\left\{s_n^{\rm qua} : n = 1, \ldots, \tilde{N}\right\} := \left\{s_m^{\rm geo} : m = 1, \ldots, M\right\} \cup \left\{s_n^{\rm col} : n = 1, \ldots, N\right\}.$$

Now the quadrature rule for the computation of I is the composite rule

$$I = \sum_{n=1}^{\tilde{N}} \int_{s_n^{\rm qua}}^{s_{n+1}^{\rm qua}} k(t,s)\varphi(s){\rm d}s \sim \sum_{n=1}^{\tilde{N}} \sum_{l=1}^{l_n} k\Big(t, s_n^{\rm qua} + \tau_l^{l_n} \triangle s_n\Big)\varphi\Big(s_n^{\rm qua} + \tau_l^{l_n} \triangle s_n\Big) w_l^{l_n} \triangle s_n,$$
$$\triangle s_n := [s_{n+1}^{\rm qua} - s_n^{\rm qua}],$$

where $\int_0^1 f(s){\rm d}s \sim \sum_{l=1}^{l_n} f(\tau_l^{l_n}) w_l^{l_n}$ is the Gauss-Legendre rule of order l_n. The orders l_n are chosen between a minimal value $l_{\min} = 2$ or 3 and a maximal value $l_{\max} = c_1 + 2\log N$ with a suitable constant c_1. Most of the the intervals $[s_n^{\rm qua}, s_{n+1}^{\rm qua}]$ are far from the singularity point t of function k, and we can choose $l_n = l_{\min}$. On the other hand, for the intervals $[s_n^{\rm qua}, s_{n+1}^{\rm qua}] \subseteq [s_{n'}^{\rm col}, s_{n'+1}^{\rm col}]$ with $t \in [s_{n'}^{\rm col}, s_{n'+1}^{\rm col}]$, we choose the maximal $l_n = l_{\max}$. On intervals $[s_n^{\rm qua}, s_{n+1}^{\rm qua}] \subseteq [s_{n''}^{\rm col}, s_{n''+1}^{\rm col}]$ with $[s_{n''}^{\rm col}, s_{n''+1}^{\rm col}]$ adjacent or close to $[s_{n'}^{\rm col}, s_{n'+1}^{\rm col}]$, we reduce l_n linearly with the distance to $[s_{n'}^{\rm col}, s_{n'+1}^{\rm col}]$, i.e., we set $l_n := \max\{l_{\min}, l_{\max} - 2|n'' - n'|\}$.

4 Preconditioning of the system of linear equations

For a very accurate determination of the grating efficiencies or for problems with large ratios period over wavelength, a fine discretization is needed. Hence, large systems of linear equations must be solved. Moreover, in contrast to the sparse matrices of the finite element methods, the matrices in the systems of linear equations of boundary element methods are densely populated. Special techniques for sparse systems do not apply. Consequently, the use of direct solvers requires huge amounts of computing time. Alternatively, iterative solvers like, e.g., the GMRES method [24] converge slowly for ill-conditioned matrix equations or even diverge. Unfortunately, the boundary element matrices are ill-conditioned. The large condition numbers are attributed, on the one hand, to the non-zero orders of the integral operators (order of pseudodifferential operators acting in the scale of Sobolev spaces) and, on the other hand, to the high wave numbers, i.e., to the oscillatory behavior of the kernel functions and solutions. Especially, the high wave numbers cause serious troubles.

Clearly, to accelerate the convergence of the iterative solvers for the discretization of (2.20), a good preconditioner is needed. We denote the discretized functions, i.e., the

vector of coefficients with respect to a trial space basis, by adding the lower index N to the symbols of the original functions. Recall that N is the number of collocation points at the curves Γ_j. Similarly, we denote the discretized operators, i.e., the matrices of the finite dimensional operators with respect to a trial space basis, by adding the lower index N to the operator symbols. In other words, the matrix equation corresponding to (2.20) is

$$\begin{pmatrix} A_{1,1,N} & A_{1,2,N} \\ A_{2,1,N} & A_{2,2,N} \end{pmatrix} \begin{pmatrix} w_{1,N} \\ w_{2,N} \end{pmatrix} = \begin{pmatrix} 0 \\ u_N^i \end{pmatrix}. \tag{4.1}$$

Instead of (4.1) we solve the preconditioned equation

$$\begin{pmatrix} B_{1,1,N} & B_{1,2,N} \\ B_{2,1,N} & B_{2,2,N} \end{pmatrix} \begin{pmatrix} A_{1,1,N} & A_{1,2,N} \\ A_{2,1,N} & A_{2,2,N} \end{pmatrix} \begin{pmatrix} w_{1,N} \\ w_{2,N} \end{pmatrix} = \begin{pmatrix} B_{1,1,N} & B_{1,2,N} \\ B_{2,1,N} & B_{2,2,N} \end{pmatrix} \begin{pmatrix} 0 \\ u_N^i \end{pmatrix} \tag{4.2}$$

iteratively, e.g., by GMRES. Clearly, (4.2) is equivalent to (4.1) if the preconditioner $(B_{i,j,N})_{i,j=1}^2$ is invertible. In order to guarantee a faster convergence of GMRES for (4.2), the entries $B_{i,j,N}$ must be chosen such that the product matrix on the left-hand side of (4.2) is better conditioned than the matrix of (4.1). Sometimes an ILU type inverse of the matrix in (4.1) is a good choice for a preconditioner. However, we have used the following preconditioner. We denote the matrix of the discrete Fourier transform FFT in the N-dimensional Euclidean space by F_N. For any $N \times N$ matrix $M = (m_{k,l})_{k,l=1}^N$ and any integer $d \geq 0$, we define $[M]_d$ by setting to zero all the entries except those of the d diagonals around the main diagonal and of the d diagonals in the left lower resp. right upper corner.

$$[M]_d := \left(m_{k,l,d}\right)_{k,l=1}^N, \qquad m_{k,l,d} := \begin{cases} m_{k,l} & \text{if } |k-l| \leq d \text{ or } |k-l \pm N| \leq d, \\ 0 & \text{else.} \end{cases}$$

Then our preconditioner is defined by

$$\begin{pmatrix} B_{1,1,N} & B_{1,2,N} \\ B_{2,1,N} & B_{2,2,N} \end{pmatrix} := \begin{pmatrix} F_N^{-1} & 0 \\ 0 & F_N^{-1} \end{pmatrix} \begin{pmatrix} [F_N A_{1,1,N} F_N^{-1}]_d & [F_N A_{1,2,N} F_N^{-1}]_d \\ [F_N A_{2,1,N} F_N^{-1}]_d & [F_N A_{2,2,N} F_N^{-1}]_d \end{pmatrix}^{-1} \begin{pmatrix} F_N & 0 \\ 0 & F_N \end{pmatrix},$$

i.e., we take the Fourier transform of the matrices $A_{i,j,N}$, we truncate upto d diagonals around the main diagonal and close to the matrix corners, and finally we choose the inverse of the truncated block matrix as a preconditioner for the Fourier transformed equation (4.1). To compute the preconditioner, we can use the Fast Fourier Transform algorithm for F_N and F_N^{-1} and fast direct solvers for matrices with only a few number of non-zero diagonals adjacent to the main diagonal.

In Table 2 we present the number of preconditioned GMRES iterations for the example introduced at the end of Section 2.4. The GMRES iteration is interrupted if the residual error is less than 10^{-14}. Table 2 shows that the iteration count remains almost bounded. For TE polarization, the corresponding It is even smaller. However, for a difficult problem

Table 2: Number of preconditioned GMRES iterations in case of a simple echelle grating.

N	graded mesh	uniform mesh
	Number of Iterations	Number of Iterations
64	44	29
128	48	30
256	50	29
512	52	29
1024	54	31
2048	53	
4096	55	

with large ratio period over wavelength, more iterations are needed. Nevertheless, preconditioned GMRES is still much faster than Gaussian elimination. For instance, the echelle grating with a grating frequency of 83 periods per mm and illuminated with a wavelength equal to 180 nm (cf. [22]) requires 292 iterations to reduce the residual error of a $2 \cdot 4\,096$ dimensional system to 10^{-8}. Note that this example is computed over uniform meshes of collocation points. All the degrees of freedom are needed to resolve the oscillations of the solution. Mesh refinement at corners reduces the error only for more than 4 096 collocation points per curve.

5 Example

A useful and demanding application is the simulation of coated echelle gratings employed in a Littrow reflection configuration which has been investigated in detail e.g. in [14].

Echelle gratings are blazed gratings possessing an asymmetrical triangular groove shape with an apex angle of 90°. They are coarse, but precisely manufactured gratings used only at high spectral orders (50 to 2500) and high angles of diffraction between 63° and 80°. The small, steep facets of the triangular profile are used as working facets. In reflection they act as micro-mirrors so that when incident light is close to the direction normal to the facets, almost all of it is reflected into a direction almost opposite to that of the incidence. Under a suitable choice of grating period and wavelength this is also the direction of a diffraction order, and blazing occurs in that order. This grating configuration is called Littrow mount, and the corresponding angle of incidence is the Littrow angle θ_{L} characterized by the condition

$$\sin\theta_{\mathrm{L}} = \frac{p\lambda}{2d}$$

with wavelength λ, grating period d, and diffraction order p. The configuration is schematically depicted in Fig. 2.

A salient feature of echelles is a high angular dispersion and, possibly, a high resolution. The dispersion of echelle gratings can be as high as that of gratings with fine pitch, but,

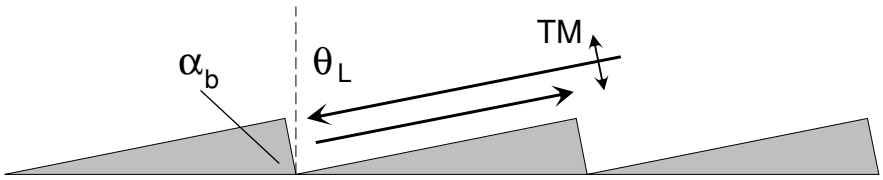

Figure 2: Echelle grating in Littrow mount: blaze angle $\alpha_b \geq 60^\circ$, apex angle equal to 90°.

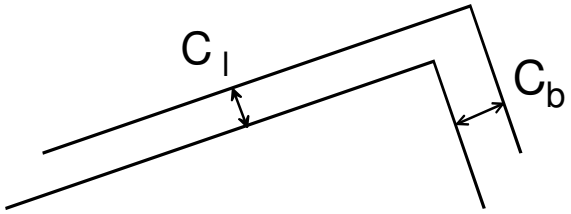

Figure 3: Coated echelle grating: different thickness of coating over the two facets of the profile.

because of the low ratio λ/d, polarization effects play a minor role. Hence, these gratings are the main tools for applications with demanding spectral resolution (cf. e.g. [16]). Echelles are also employed as external resonator cavity diffraction gratings in high power laser applications. Because of the high angular dispersion, they are the main components for narrowing the desired laser line. Due to the high power density, the gratings are prone to damage and the extension of lifetime is an important issue. One way to improve lifetime is to minimize energy absorption in the grating while preserving a maximal efficiency in the working order. To realize this, aluminium echelles coated with dielectric protective layers of different thickness over the two facets (cf. Fig. 3) have been proposed and optimized in [14]. Of course, the optimization has been based on a rigorous electromagnetic simulation. By C_b we denote the coating thickness on the blaze facet and by C_l that on the long facet which is the anti-blaze facet. Both thicknesses are measured perpendicular to the facet planes.

While in both cases, TE and TM polarization, the thickness C_b can be optimal with respect to a maximal efficiency and with respect to minimal absorption at the same time, this is not the case for the optimization of C_l. This can be seen in Figs. 4 and 5 for TE and TM polarization, respectively. In other words, it is only possible to optimize the pair of coating thicknesses of the layer with respect to one of the two objectives.

A further important observation is that a wrong choice of coating thickness on the anti-blaze facet can significantly reduce efficiency and increase absorption due to a resonance anomaly. The grazing incidence to the metallic anti-blaze facet together with a specific thickness of the dielectric coating couples guided waves into the coated grating. The coating thickness for which the resonance anomaly occurs can be deduced by e.g. rigorous calculations (see Fig. 4 for a coating thickness of 37 nm on the anti-blaze facet and Fig. 5 for

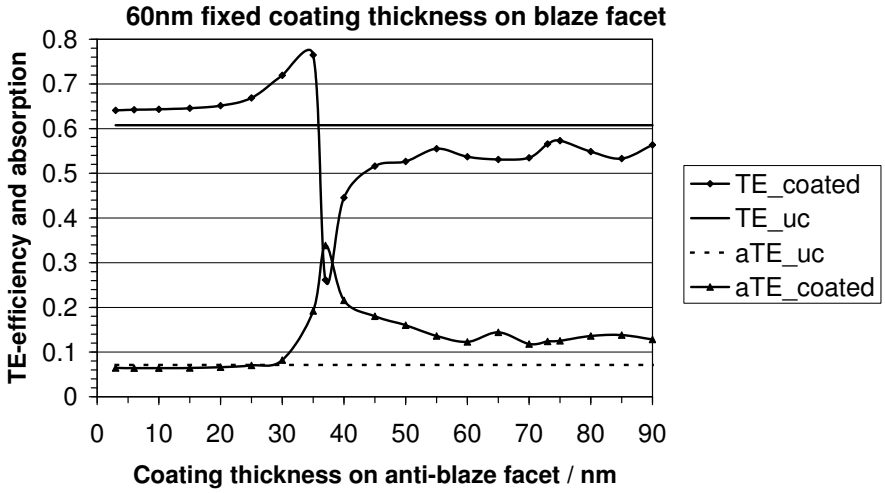

Figure 4: TE efficiency (TE_coated) in the -122^{nd} diffraction order and TE absorption (aTE_coated) depending on C_l: MgF_2 coated aluminium echelle grating, $C_b = 60$ nm. For comparison: TE efficiency (TE_uc) and TE absorption (aTE_uc) for uncoated grating.

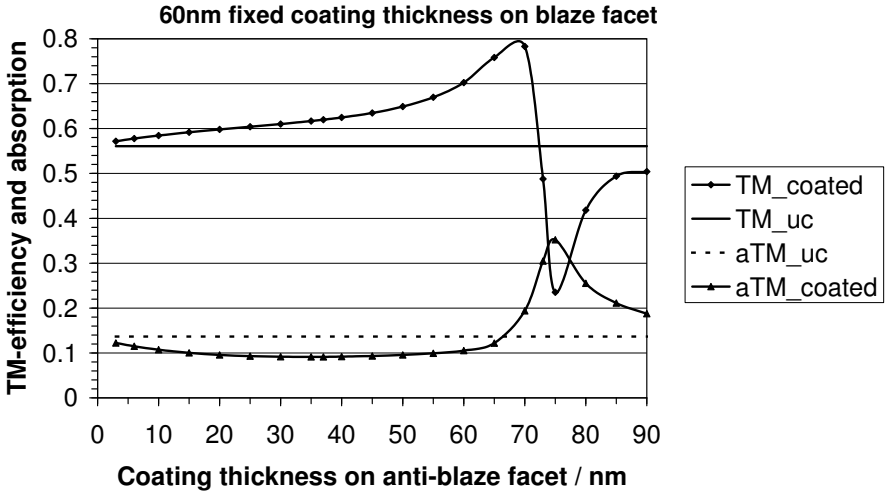

Figure 5: TM efficiency (TM_coated) in the -122^{nd} diffraction order and TM absorption (aTM_coated) depending on C_l: MgF_2 coated aluminium echelle grating, $C_b = 60$ nm. For comparison: TM efficiency (TM_uc) and TM absorption (aTM_uc) for uncoated grating.

a coating thickness of 73 nm on the anti-blaze facet). Now the coating can be adjusted to avoid these critical values. Moreover, coatings thinner than the resonance values by only a few nanometers maximize the efficiency. If the coating deposition process is technologically highly developed, the efficiency can be improved by up to 20 basis points compared to a simple coating. So, the protective layer improves the properties of the bare echelle.

For the numerical evaluation, we compare the spline collocation method (SC) described in the present publication with the method of the first version of the package IESMP (cf. [13, 20]) which is based on the hybrid discretization scheme (H) described in Section 2.4.

The blaze angle α_{b}, which is also the Littrow angle θ_{L}, is 78.7°. Hence, the incidence is normal to the small, steep echelle facets so that they can act as micro-mirrors. Our calculations are performed for the excimer laser wavelength $\lambda = 193.35$ nm and grating period $d = 12.0285\,\mu$m corresponding to 83.136 lines/mm. In this case, the working order is the -122^{nd} diffraction order, which is diffracted backward to the direction of incidence. Due to a ratio of $d/\lambda = 62$ and the fact that profile edges and small coating thicknesses have to be treated, the example is quite demanding. Aluminium is used as the reflecting material of the grating [16] due to the high reflectivity for the given wavelength. Indeed, it has a complex refractive index of $\nu = 0.113 + \mathrm{i}2.208$ for the above given wavelength. Since aluminium creates a natural protection layer of Al_2O_3, the fast-fired aluminium layer is immediately coated by an MgF_2 layer to prevent oxidization (cf. [16]). Often the laser source is linearly polarized, so that either TE polarization or TM polarization is considered here. As done in [14] for the first time, we also consider an independent choice of the coating thickness $\mathrm{C_b}$ on the blaze facet and of the thickness $\mathrm{C_l}$ on the long facet of the echelle grating. The refractive index of the dielectric coating material MgF_2 is $\nu = 1.44$.

Fixing the coating thickness $\mathrm{C_b}$ to 60 nm, we let $\mathrm{C_l}$ vary between 3 nm and 90 nm to study the resonance effects. The results presented in Figs. 4 and 5 are calculated with method (SC) using $N = 2048$ discretization points without mesh refinement at the edges because of the large ratio d/λ. A comparison of the same method with only $N = 1024$ discretization points in Fig. 6 shows deviations smaller than 1-2% which is sufficient for practical requirements. Similar calculations with the older method (H) using $N = 1024$ result in deviations smaller than 1% for the efficiency and smaller than 5% for the absorption as long as the coating thickness $\mathrm{C_l}$ is larger than 5 nm. For e.g. $\mathrm{C_l} = 3$ nm, the deviation of the TM efficiency is 12% and the absorption could not be determined because the sum of efficiencies is larger than 1. Nevertheless, the results of method (H) with $N = 2048$ discretization points differ from those of method (SC) with $N = 2048$ by less than 3% for $\mathrm{C_l} = 3$ nm and less than 1% for larger thicknesses. Hence, in this application with a relatively large value $\mathrm{C_b}$, method (SC) can be used with $N = 1024$ discretization points and satisfies the practical requirements. Also method (H) can be used with $N = 1024$ discretization points resulting in an accuracy sufficient for practical use. Only for thicknesses smaller than $\mathrm{C_l} = 6$ nm, $N = 2048$ discretization points are needed.

Now, using the new method (SC), the effects of the natural protection layer of Al_2O_3 with the refractive index $\nu = 1.78 + \mathrm{i}0.001$ on top of the above grating type can be investigated. The coating thicknesses $\mathrm{C_l}$ as well as $\mathrm{C_b}$ are chosen from the set $3, 6, 10, 15, 20, 25$ so that calculations for 36 combinations are to be performed. A typical result with equal thicknesses on both facets using $N = 2048$ discretization points is given in Fig. 7. A

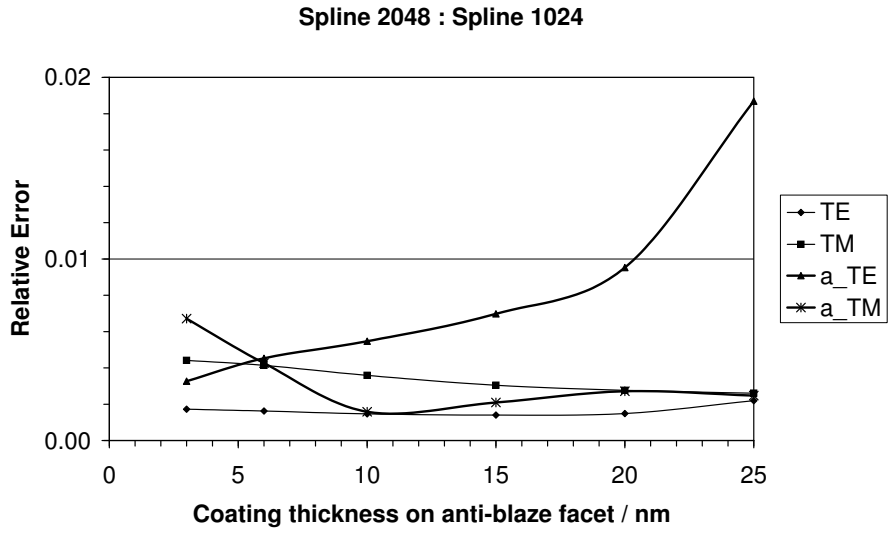

Figure 6: Relative error of polarization dependent efficiency and absorption: $C_b = 60$ nm, small C_l, MgF_2 coated aluminium echelle grating. The error is deviation of approximate efficiencies with $N = 1024$ and $N = 2048$ discretization points of the (SC) method.

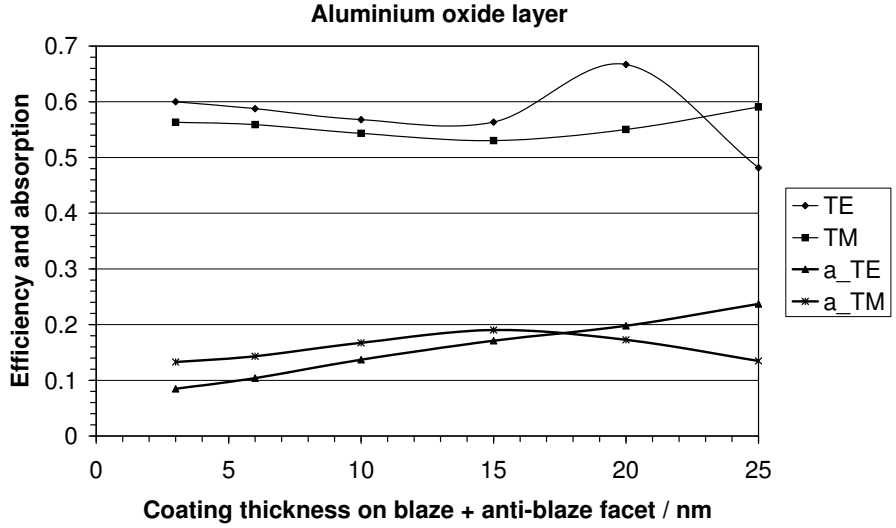

Figure 7: Polarization dependent efficiency in the -122^{nd} diffraction order and absorption (a_TE, a_TM): $C_b = C_l$, Al_2O_3 coated aluminium echelle grating, natural protection layer.

comparison with results of the same method (SC) using only $N = 1024$ discretization points in Fig. 8 shows deviations smaller than 5% which would be sufficient for practical use. Similar results hold for all other combinations of coating thicknesses independently on whether the values of C_b or C_l are small or large. A comparison using $N = 1024$

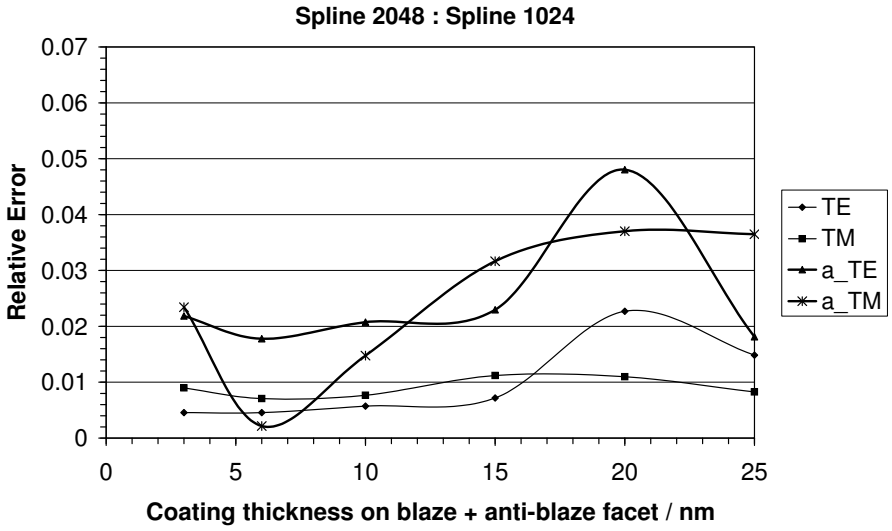

Figure 8: Relative error of the polarization dependent efficiency and absorption (a_TE, a_TM): $C_b = C_l$, Al_2O_3 coated aluminium echelle grating, natural protection layer. The error is between $N = 1024$ and $N = 2048$ discretization points of the (SC) method.

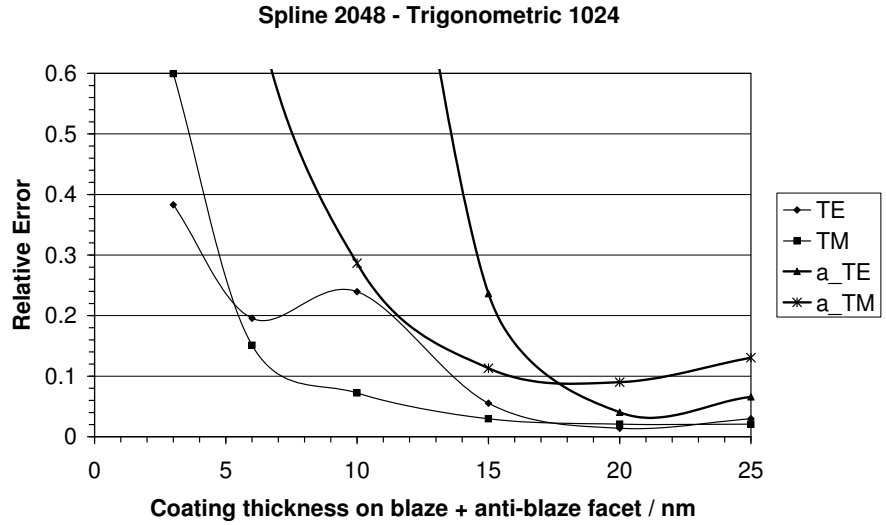

Figure 9: Relative error of the polarization dependent efficiency and absorption (a_TE, a_TM): $C_b = C_l$. Al_2O_3 coated aluminium echelle grating. The error is between $N = 1024$ and $N = 2048$ discretization points of the (H) method.

discretization points for the older method (H) and $N = 2048$ discretization points of the (SC) method results in relatively large deviations. For the example with equal thicknesses on both facets, the deviation plots of these calculations can be found in Fig. 9, the relative errors are up to 20% if the coating thicknesses are 15 nm and they grow significantly if

the thicknesses shrink. In particular, if one of the coating thicknesses is 10 nm or less, then the efficiency error grows from 15% to 60% and the accuracy of the approximate absorption values is not acceptable. In general, the simulation for a small thickness on the blaze facet is more challenging than a small thickness of the same size on the anti-blaze facet.

Hence, for this second application, method (SC) can be used with $N = 1024$ discretization points in all practical cases and yields an accuracy sufficient for practical requirements. In contrast to this, method (H) cannot be used with $N = 1024$ discretization points since most of the approximate values are inaccurate and not acceptable. Even with $N = 2048$ method (H) can be used safely only under the restrictions $C_b \geq 15$ nm and $C_l > 25$ nm. Otherwise one has to check whether, for the actual pair of thicknesses, the approximation is acceptable or not.

Now let us compare the computation times of the considered methods (SC) and (H) based on the same kernel function evaluations and on GMRES iterations upto an accuracy of 10^{-10}. The solution of the problem with coating thickness $C_l = 60$ nm by the method (SC) with $N = 1024$ on an AMD Opteron, 2.6 GHz, required about 692 seconds with the major part of 651 seconds for the computation of the kernel functions. This relatively huge amount is caused by the high wave number and the presence of thin layers in our problem. Since the computations of the kernel functions can be performed in parallel, a considerable speed up of the program is possible. The preconditioned GMRES needs 140 and 117 iterations for solving the linear systems in TE and TM polarization, respectively, which took 18 seconds. Setting the computation time for method (SC) with $N = 1024$ to 100%, method (SC) with $N = 2048$ is accomplished in 340% of the time, while (H) with $N = 1024$ and $N = 2048$ requires 40% and 170% of the time, respectively. We recommend the following rule for switching between (SC) and (H) and for choosing N the number of discretization points. If possible, use method (H) with $N = 1024$. This is the fastest choice, and often the results are sufficiently accurate from the practical point of view. If this is not the case, then switch to (SC) but retain N. This costs a factor 2.5 in computation time, only. In the case that the results are still not sufficiently accurate, switch back to method (H), but now double the number N. Finally, in the rare case of inaccurate results for method (H) and doubled N, method (SC) with doubled N is to be chosen. In any case, for small C_b and C_l, method (SC) is to be used right from the start.

Our next remark concerns the iteration scheme GMRES. With the preconditioning described in Section 4, we are now in the position to solve the equations arising from coated gratings iteratively. This was, for a long time, not possible because of the ill-conditioned matrices. The implementation of the preconditioned GMRES reduces the solution time of the 1024×1024 linear system to 1/6 of the time needed with Gaussian elimination. For $N > 1024$, this reduction is even more pronounced.

Already the old IESMP ([20], [13]) has been applied to design, development, and quality control in the grating production at Carl Zeiss Jena since 1985. The new IESMP is more flexible, more accurate and more stable. If the numerical error due to corner singularities is dominating, then the new IESMP is even faster than the old one. Again,

the application of the method will be design, research, development, and quality control.

Acknowledgments

Part of the presented work has been supported by the German Federal Ministry of Education and Research under Grant number 13N 8478.

References

[1] T. Abboud and J. C. Nedelec, Electromagnetic waves in an inhomogeneous medium, J. Math. Anal. Appl., 164 (1992), 40–58.
[2] G. Bao, Finite element approximation of time harmonic waves in periodic structures, SIAM J. Numer. Anal., 32, (1995), 1155–1169.
[3] G. Bao, Z. Chen and H. Wu, An adaptive finite element method for diffraction gratings, J. Opt. Soc. Am. A, 22 (2005), 1106–1114.
[4] A.-S. Bonnet-Bendhia and F. Starling, Guided waves by electromagnetic gratings and non–uniqueness examples for the diffraction problem, Math. Meth. Appl. Sci., 17 (1994), 305–338.
[5] X. Chen and A. Friedman, Maxwell's equations in a periodic structure, Transactions AMS, 323 (1991), 465–507.
[6] J. Chandezon, D. Maystre and G. Raoult, A new theoretical method for diffraction gratings and its applications. J. Opt. (Paris), 11 (1980), 235–241.
[7] D. Colton and R. Kress, Inverse Acoustic and Electromagnetic Scattering Theory, Applied Mathematical Sciences 93, Springer Verlag, Berlin Heidelberg, 1992.
[8] J. Elschner, R. Hinder and G. Schmidt, Finite element solution of conical diffraction problems, Adv. Comput. Math., 16 (2002), 139–156.
[9] J. Elschner and G. Schmidt, Diffraction in periodic structures and optimal design of binary gratings I. Direct problems and gradient formulas, Math. Meth. Appl. Sci., 21 (1998), 1297–1342.
[10] L. I. Goray, Modified integral method for weak convergence problems of light scattering on relief grating, in: R. I. Sutherland, D. W. Prather, and I. Cindrich (Eds.), Diffractive and Holographic Technologies for Integrated Photonic Systems, Proc. SPIE, 4291 (2001), 1–12.
[11] L. I. Goray, Numerical analysis of the efficiency of multilayer-coated gratings using integral method, Nucl. Instrum. Meth. Phys. Res. A, 536 (2005), 211–221.
[12] L. I. Goray and S. Yu. Sadov, Numerical modelling of coated gratings in sensitive cases, OSA TOPS, 75 (2002), 356–379.
[13] B. H. Kleemann, Elektromagnetische Analyse von Oberflächengittern von IR bis XUV mittels einer parametrisierten Randintegralmethode: Theorie, Vergleich und Anwendungen, Dissertation, TU Ilmenau, 2002, Mensch und Buch Verlag Berlin, 2003.
[14] B. H. Kleemann and J. Erxmeyer, Independent electromagnetic optimization of the two coating thicknesses of a dielectric layer on the facets of an echelle grating in Littrow mount, J. Mod. Optic, 51 (2004), 2093–2110.
[15] C. M. Linton, The Green's function for the two-dimensional Helmholtz equation in periodic domains, J. Eng. Math., 33 (1998), 377–402.
[16] E. G. Loewen and E. Popov, Diffraction Gratings and Applications, Marcel Dekker New York, 1997.

[17] F. Matta and A. Reichel, Uniform computation of the error function and other related functions, Math. Comput., 25 (1971), 339–344.
[18] D. Maystre, Integral methods, in: R. Petit (Ed.), Electromagnetic Theory of Gratings, Springer-Verlag, Berlin, 1980, pp. 63–100.
[19] M. G. Moharam and T. K. Gaylord, Rigorous coupled wave analysis of planar grating diffraction, J. Opt. Soc. Am., 71 (1981), 811–818.
[20] A. Pomp, The integral method for coated gratings: Computational cost, J. Mod. Optics, 38 (1991), 109–120.
[21] G. P. M. Poppe and C. M. J. Wijers, Algorithm 680: Evaluation of the complex error function, ACM T. Math. Software, 16(1) (1990), p. 47.
[22] E. Popov, B. Bozhkov, D. Maystre and J. Hoose, Integral methods for echelles covered with lossless or absorbing thin dielectric layers, Appl. Optics, 38 (1999), 47–55.
[23] D. W. Prather, M. S. Mirotznik and J. N. Mait, Boundary integral methods to the analysis of diffractive optical elements, J. Opt. Soc. Am. A, 14 (1997), 34–42.
[24] Y. Saad and M. H. Schultz, GMRES: A generalized minimal residual algorithm for solving nonsymmetric linear systems, SIAM J. Sci. Stat. Comput., 7 (1986), 856–869.
[25] S. Yu. Sadov, Computation of quasiperiodic fundamental solution of Helmholtz equation, in: I. Gyori, G. Ladas and S. Elaydi (Eds.), Advances in Difference Equations, Gordon and Breach, 1997, pp. 551–558.
[26] C. Schwab, Variable order composite quadrature of singular and nearly singular integrals, Computing, 53 (1994), 173–194.
[27] H. P. Urbach, Convergence of the Galerkin method for two-dimensional electromagnetic problems, SIAM J. Numer. Anal., 28 (1991), 697–710.
[28] S. Venakides, M. A. Haider and V. Papanicolaou, Boundary integral calculations of two-dimensional electromagnetic scattering by photonic crystal Fabry-Perot structures, SIAM J. Appl. Math., 60(5) (2000), 1686–1706
[29] M. Yeung and E. Barouch, Electromagnetic scatterometry applied to in-situ metrology, Proc. SPIE, 4344 (2001), 484–495.